Dissolution Kinetics of Particulate Graphite Injected into Iron/Carbon Melts

J. K. WRIGHT and B. R. BALDOCK

An experimental investigation was undertaken to study the kinetics of graphite dissolution in gas-stirred iron/carbon melts. Laboratory apparatus was developed to allow the injection of closely sized graphite into the bottom of a 1 kg scale reactor with nitrogen as a carrier gas. The effects of gas flow, particle loading, particle size, bath sulfur, and temperature on the rate of dissolution were assessed. It was found under the experimental conditions used that the graphite dissolution rate kept pace with the injection rate up to approximately 85 pct of carbon saturation, except when sulfur is present in the bath, in which case the dissolution rate is retarded. Modeling the rate of graphite particle dissolution supports the experimental results in that particle dissolution occurs quickly and under mass transport limitations. Computer generated gas-stirred flow field diagrams for the experimental reactor indicate that conditions exist for particle entrainment in the bath, and hence complete contact with the melt at all times during dissolution.

I. INTRODUCTION

TURBULENT molten iron/carbon alloys are highly reducing and provide effective heat and mass transfer media. If air or oxygen are blown onto or into an iron/carbon melt an exothermic reaction occurs in which the oxidation of dissolved carbon to carbon monoxide is extremely rapid at temperatures in excess of 1300 °C. If coal or other carbonaceous material is added to the melt the strong affinity of molten iron for carbon ensures efficient solubilization. The simultaneous dissolution of carbon and the oxidation of the dissolved carbon by oxygen injection forms the basis of a number of proposed iron bath coal gasification and ferrous smelting processes.[1,2] The addition of auxiliary fuel in the form of solid carbonaceous materials to oxygen steelmaking converters to increase scrap melting capacity is also being actively pursued.[3,4]

The most appropriate carburizing agent is, of course, coal, added either as lumps or injected as fines. The dissolution behavior of coal is highly complex, involving the rapid evolution of volatiles under flash heating conditions, perhaps particle breakup and the dissolution of the remaining pyrolyzed char. In order to avoid these complications, the present work considered the dissolution kinetics of non-volatile particulate graphite injected into iron/carbon baths. The reaction and dissolution of coals is being assessed in continuing work.

II. PREVIOUS GRAPHITE DISSOLUTION STUDIES

The majority of previous experimental graphite dissolution investigations have concentrated on the use of stationary or rotating graphite rods immersed in Fe/C melts.[5-10] All these studies concluded that graphite dissolution is governed by mass transfer in which diffusion of carbon in a liquid boundary layer at the graphite surface is rate controlling. It is also generally agreed that sulfur in molten iron, even at relatively low levels, depresses graphite dissolution rates. There is some disagreement, however, as to whether the retarding effect of dissolved sulfur is due to mass transfer or chemical limitations.

Little work has been done on the dissolution kinetics of particulate carbon in Fe/C melts. Wright and Denholm[2,11] investigated the dissolution rates of batch additions of particulate graphite, petroleum coke, and brown coal char to gas stirred Fe/C melts. It was found that the rates were mass transfer controlled, and increased with increase in the gas stirring power input. This work also showed the retarding effect of bath sulfur on the carbon dissolution rates. Lehner[12] injected carbon powder into 6 tonne steel melts and found that mass transport under the conditions used is so fast that carbon assimilation matched the feed rate.

III. GAS/PARTICLE INJECTION CONSIDERATIONS

The subsurface injection of gases into liquids has been the subject of many studies and although some aspects are still not well understood, two regimes of gas behavior have been established—bubbling and jetting flow. In the bubbling flow regime (injection velocities less than sonic), the gas emerges from the orifice as a regular series of bubbles characterized by the formation, growth, and pinching-off of the gas envelope stem at the outlet. As the flowrate is increased, a continuous gas channel is formed, at least in the vicinity of the orifice, and the pinching-off effect is either negligible or occurs at extremely short intervals. Farther downstream, under the effect of turbulent entrainment, the jet disintegrates into a swarm of smaller gas bubbles. The steady jet flow regime is observed under conditions where the momentum forces of the gas stream are larger than the buoyancy forces acting on the gas bubbles.

When solids are added to a gas stream, because the densities of the solids are three or more orders of magnitude larger than those of the gas, gases containing entrained particles have an increased momentum over particle-free gases. As a result, jetting is generally observed at lower gas flow-

J. K. WRIGHT is Senior Principal Research Scientist, CSIRO, Division of Mineral Engineering, Melbourne, Australia. B. R. BALDOCK, formerly Experimental Scientist, CSIRO, Division of Mineral Engineering, is Development Metallurgist, AUSMELT Pty. Ltd., Melbourne, Australia.

Manuscript submitted January 2, 1987.

rates than in gas only injection. However, the prediction of the transition between the two regimes is much more complex than for gas only flows as the properties of a third phase must be considered.

A number of investigations have physically modeled the injection of powders into liquids under a variety of conditions.[13–17] Most of these investigations showed that the gas and powder separates quickly after injection with the particles left in intimate contact with the liquid phase.

Farias and Robertson[18] developed a criterion to predict the transition from bubbling (gas/particle separation) and jetting (particles and gas flowing together into the liquid). The "entrainment number" (*Ne*) characterizing the bubble/jetting transition was given as:

$$Ne = 0.75(M_p h \rho_g)/(M_g D_p \rho_l)$$

where M_p = mass flow of solids in the gas stream
M_g = mass flow of gas
h = bubble height (equivalent to bubble diam.)
D_p = particle diam.
ρ_g = gas density
ρ_l = liquid density

If *Ne* was below 3, bubbling behavior was observed, while for *Ne* in excess of 4.5, jetting was observed. Jetting is favored by high particle loadings and small particle size. Irons and Tu[19] also found that the particle size and loading affects the bubbling/jetting transition. With high loadings and fine particle sizes, the gas and particles travel at about the same rate such that most of the gas flows with the particles in a coupled state. After contact with the liquid, the gas/particle stream continues to flow in a coupled state, at least in the vicinity of the tuyere, so forming a gas/particle/liquid jet. At low loadings the gas is uncoupled and forms bubbles through which the particles flow and can penetrate the gas envelope and enter the liquid.

Farias and Irons[20] have produced a diagram summarizing the different possible regimes of gas/powder injection into liquids. This diagram is reproduced in Figure 1. The diagram shows the various regimes to be expected as a function of gas velocity, particle size, and type. This diagram will be referred to later in a discussion of the experimental injection conditions used.

IV. MATERIALS

The testwork was conducted using crushed and closely sized high purity electrode graphite. The proximate analysis of graphite was 96.75 pct fixed carbon, 0.98 pct volatiles, 2.27 pct ash, 0.24 pct moisture.

The graphite was crushed and screened into a number of different size fractions. Dissolution tests were done on 355 to 106, 495 to 358, and less than 106 micrometer particles. The particle density of the graphite of 1.6 g · cm^{-3} was calculated by weighing particle batches, coating the particles with wax dissolved in benzene, and measuring the particle volume by water displacement.

V. APPARATUS AND EXPERIMENTAL PROCEDURE

A schematic diagram of the experimental apparatus is shown in Figure 2. Iron/carbon melts were prepared from

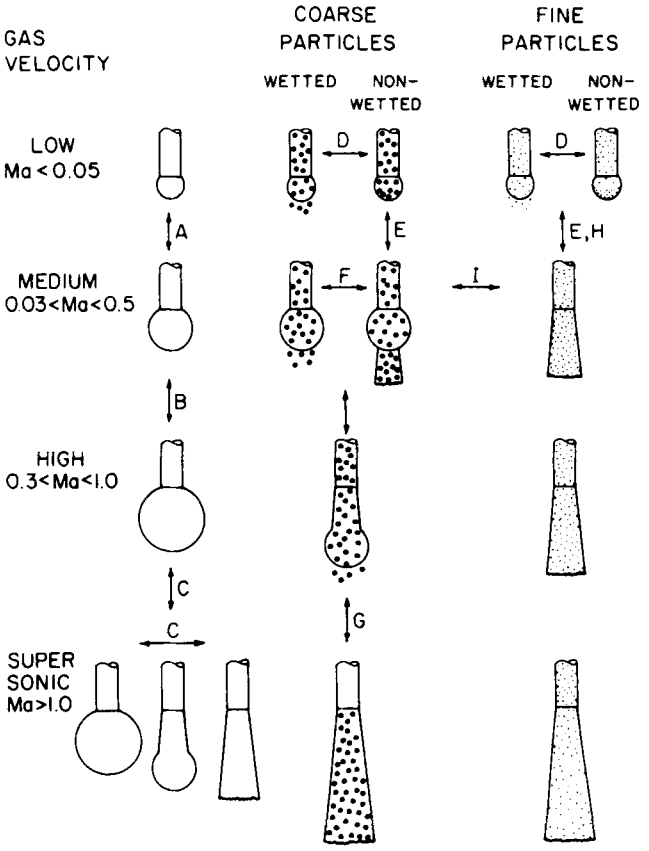

Fig. 1—Summary of the different possible regimes in injection of gas-powder mixtures into liquids.[20]

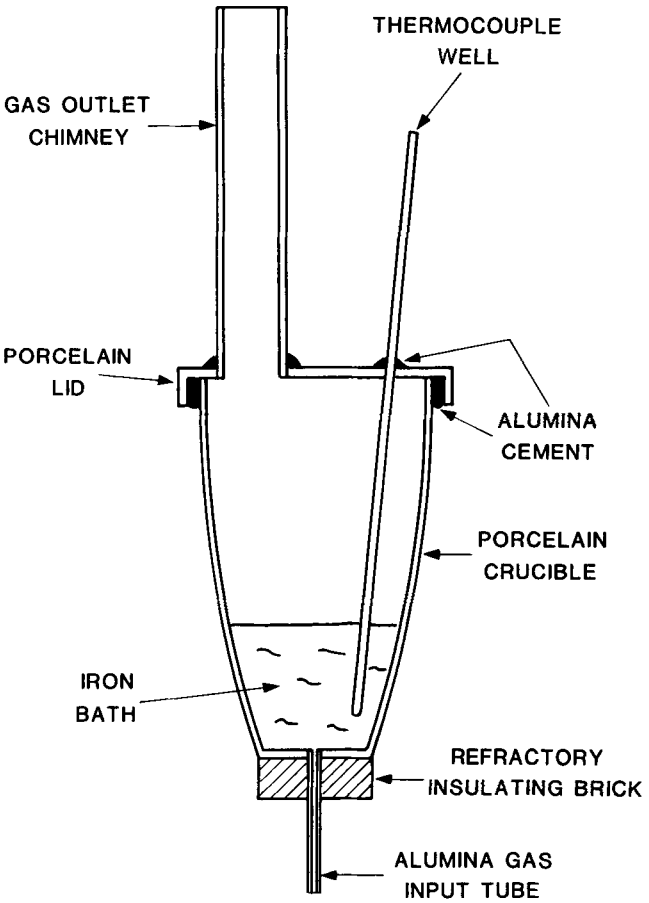

Fig. 2—Schematic diagram of the bottom-blown crucible.

electrolytic iron and high purity electrode graphite. The Fe/C charges (1000 g containing 2 pct carbon) were contained in lidded porcelain crucibles equipped with an offset gas outlet chimney. Nitrogen/graphite was injected into the melt through 2 mm I.D. alumina tubes which were cemented into the bottom of the crucibles using high alumina ("Corline") refractory cement. This assembly was placed inside an enclosure made from two silicon carbide crucibles (with their wider, open ends together) which acted as susceptors for a 40 kW, 10 kHz induction furnace.

The experimental procedure involved heating the iron/graphite mixtures at a rate of approximately 5 °C/min under the control of a HP 85/3421A data acquisition and control unit until the desired test temperature (1400 to 1500 °C) was reached. A nitrogen gas flow of approximately 1 liter/min through the bottom port was maintained at all times to prevent oxidation by infiltrate air and to prevent the melt running back down the injection port.

Particulate graphite was metered into the reactor using a pressurized feeder consisting of a hopper, in which the solids are mechanically agitated, placed above a speed-controlled conveyer belt. The solids fall through a feed gate onto the belt and are transported into an outlet orifice where they become entrained in the nitrogen carrier gas and are delivered to the iron bath *via* 2 mm I.D. high pressure nylon tube. The feeder is capable of accurately metering 2 to 20 g of graphite per minute.

Once the melt temperature had stabilized at the controlled set point, the nitrogen injection rate was increased to the desired level and solids feeding was commenced by starting the conveyer belt at a predetermined rate. Bath samples were taken from the melt at fixed intervals throughout the injection period using silica suction tubes. The melt samples were later analyzed for total carbon using a "Leco" combustion analyzer. In all tests, the carbon content of the bath was increased from about 2 pct to saturation at the reaction temperature.

VI. EXPERIMENTAL INJECTION CONDITIONS

The majority of the graphite/coal injection tests were conducted under the conditions shown in Table I.

Applying Farias and Robertson's injection number criterion,

$$Ne = 0.014 \text{ to } 0.068$$

This is well below 3, the transition parameter, and indicates that the injection system was operating in the bubbling regime. Similar calculations using criteria of Irons and Tu[19] and Kimura[21] also led to the conclusion that under the injection conditions used, the gas/powder jets did not penetrate deeply into the melt but rather bubbles were formed at the tuyere exit.

Table I. Conditions for Graphite Injection Tests

Bath weight	1 kg
Bath depth	0.058 m
Tuyere I.D.	0.002 m
Nitrogen carrier gas flow	4 to 6 liters/min
Graphite feed rate	2 to 20 g/min
Particle size	106 to 495 micrometers
Particle fraction	0.31×10^{-3} to 3.1×10^{-3}
Mass fraction	0.3 to 4.2

The particles passing into the bubbles can either penetrate the bubble surfaces or be retained at the interface. A number of correlations are available in the literature which allow calculation of critical particle velocities for penetration of liquid surfaces.[22–26] The correlations of Voronova[22] and Ozawa,[26] representing the minimum and maximum penetration velocities, are shown in Figure 3. In order to use this information, the particle velocities in the experimental work are required. As the particle velocities were not directly measured, estimates were made using hydraulic transport correlations derived by Chandok and Pei[27] and Soo.[28] The calculation method is given in the appendix.

The calculated particle to gas velocity ratios (U_p/U_g) varied from 1 to 0.88 depending on the injection conditions used. In general, the ratio decreased with increasing particle size and mass loading. The calculated particle velocities are plotted in Figure 3 where it can be seen that for average particle sizes in excess of 230 micrometers, the velocities are significantly above the predicted critical velocities. For the lower particle size used (assumed average of 53 micrometers), the particle velocity is lower than the critical velocity predicted by the Ozawa relation assuming a wetting angle of 180 deg, but still well above the Voronova prediction. From these results it is reasonable to assume that the particles penetrate the bubble surface under the injection conditions employed and would give rise to the flow regime *F* for wetted particles illustrated in Figure 1. Under these conditions, the particles separate from the gas stream close to the tuyere and penetrate the bubble envelope, thus ensuring intimate contact with the liquid iron.

VII. RESULTS

A complete listing of the test conditions employed is presented in Table II.

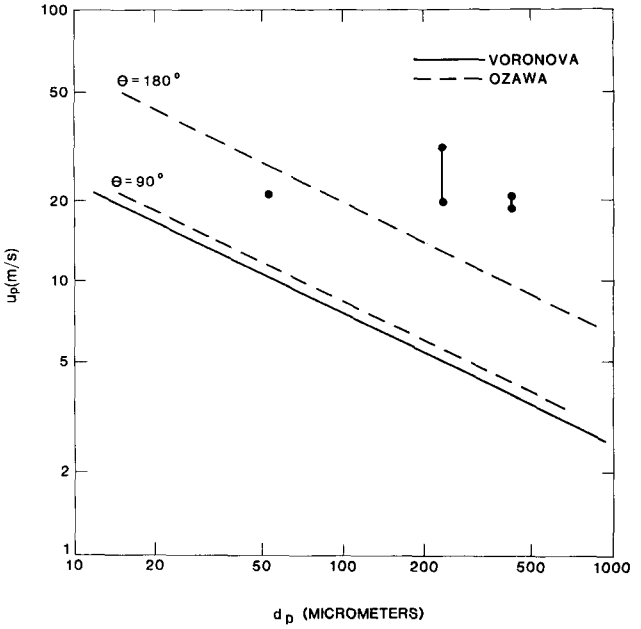

Fig. 3—Comparison of calculated experimental particle injection velocities with critical penetration velocity correlations.

Table II. Experimental Injection Tests (2 mm Tuyere, Nitrogen Carrier Gas)

Solids Feedrate (g/min)	Carrier Gas (l/min)	Particle Size (Micrometers) Graphite	Bath Temp. (°C)	Bath S Conc. Nom. (Pct)
1.6	4	355 × 106	1450	—
3.4	4	355 × 106	1450	—
7.2	4	355 × 106	1450	—
19.9	4	355 × 106	1450	—
4.0	4	355 × 106	1400	—
4.0	4	355 × 106	1500	—
2.0	4	355 × 106	1450	—
2.0	4	495 × 355	1450	—
4.0	4	495 × 355	1450	—
2.0	4	−106	1450	—
4.0	4	−106	1450	—
2.0	6	355 × 106	1450	—
4.0	6	355 × 106	1450	—
4.0	4	355 × 106	1450	0.1
4.0	4	355 × 106	1450	0.5
4.0	4	355 × 106	1450	1.0

A. *Effect of Feedrate*

Plots of bath carbon concentration against time for 355 × 106 μm graphite at injection rates of 1.6 to 19.9 g/min are shown in Figure 4. The measured carbon concentrations are shown as experimental points while the actual carbon feed rates are shown as solid lines. These plots show that for all the feed rates used, the rate of dissolution of the graphite was virtually identical to the rate of injection. Only at carbon concentrations approaching saturation (5.02 pct at 1450 °C), and at the higher feed rates, did the dissolution rates fall behind the injection rates.

B. *Effect of Bath Temperature*

Dissolution plots for 355 × 106 μm graphite particles (4 g/min) at 1400 and 1500 °C are shown in Figure 5. These plots show much the same trend as the feed rate

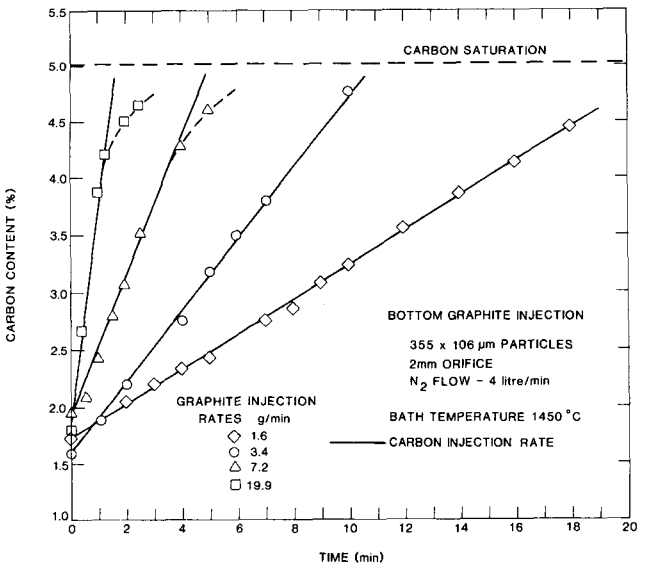

Fig. 4—Effect of feedrate on the dissolution of injected graphite.

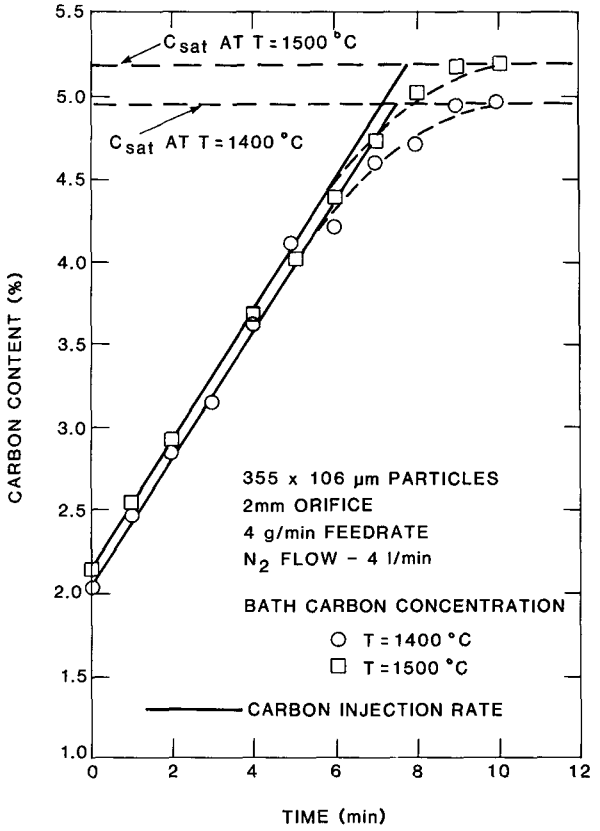

Fig. 5—Effect of temperature on the dissolution of injected graphite.

results in that the dissolution rates match the carbon injection rates up to approximately 85 pct of saturation. Bath temperature over the range 1400 to 1500 °C does not appear to have a major effect on the graphite dissolution rate under the conditions used.

C. *Effect of Particle Size*

The effect of particle size on the dissolution rate of 495 × 358 μm and −106 μm graphite particles at 1450 °C is shown in Figure 6. The results show that even for the relatively large particles (average size 426.5 μm), the dissolution rate kept pace with the injection rates up to about 85 pct of saturation. The dissolution rate of the finer particles (less than 106 μm) kept pace with the injection rate up to about 95 pct of saturation.

D. *Effect of Carrier Gas Flowrate*

Only two tests were done in which the carrier gas flowrate was varied from 4 to 6 liters/min using 355 × 106 μm particles at feed rates of 2 and 4 g/min. Again the dissolution and injection rates were virtually identical with the results for graphite injection using a carrier gas at 4 liters/min under the same conditions.

E. *Effect of Bath Sulfur Concentration*

Bath sulfur concentrations of 0.1, 0.5, and 1.0 pct were made up by the addition of iron sulfide to the melts. The results of the injection of 355 × 106 μm graphite particles at 4 g/min at sulfur levels of 0.1 pct and 1.0 pct are shown in Figure 7. The results show that the dissolution rate curves

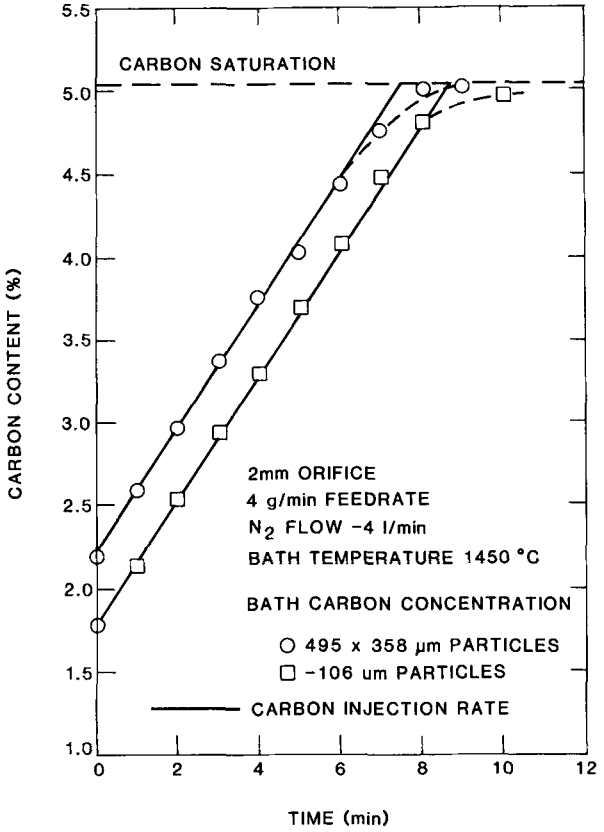

Fig. 6—Effect of particle size on the dissolution of injected graphite.

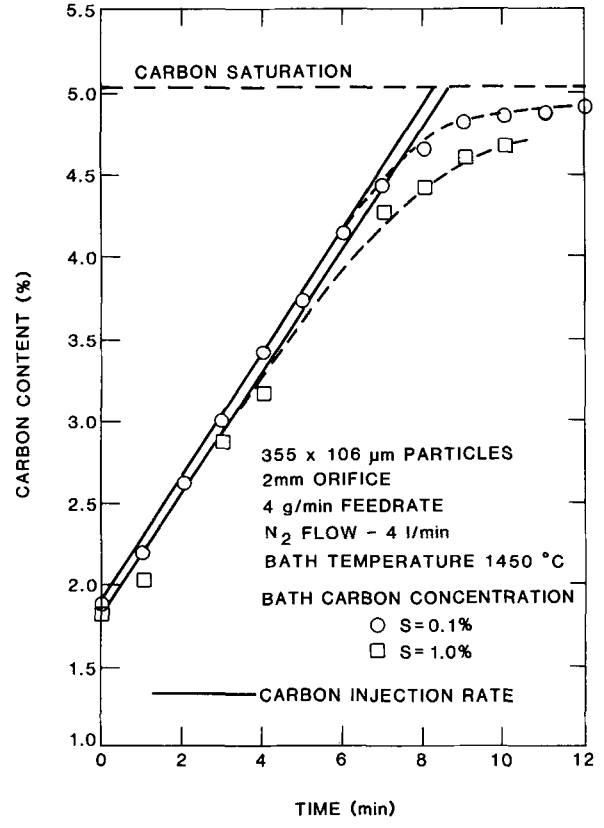

Fig. 7—Effect of bath sulfur concentration on the dissolution of injected graphite.

Table III. Effect of Sulfur on Breakaway Points

S (Pct)	Pct of Carbon Saturation
No S addition	85
0.1	87
0.5	71
1.0	62

break away from the injection rate lines at progressively lower levels of carbon concentration as the sulfur levels increase. The full results are not shown in Figure 7 for the sake of clarity; however, the breakaway points expressed as percentage of carbon saturation in the melt as a function of the melt sulfur concentration are given in Table III.

VIII. DISCUSSION

The overriding feature of all the results summarized in Figures 4 to 7 is that the graphite dissolution rates keep pace with the injection rates used over a relatively wide range of conditions. Only at carbon concentrations approaching saturation, and at high sulfur levels, do the dissolution rates start to lag the injection rates. This indicates that the graphite particles dissolve in a matter of seconds when they are injected directly into Fe/C melts with carbon concentrations less than about 85 pct of saturation.

If the dissolution process is mass transfer controlled, the change in bath carbon concentration is given by the following mass balance equation:

$$dC/dt = k(A/V)(C_s - C_b) \quad [1]$$

where k = mass transfer coefficient (cm/s)
t = time (s)
A = contact area, cm^2
V = volume of bath, cm^3
C_s = saturation carbon concentration
C_b = bulk carbon concentration

or, in terms of particle weight:

$$-dW/dt = A\rho_s V_r = A\rho_l k(C_s - C_b) \quad [2]$$

where W = particle weight (g)
V_r = rate of particle size decrease (cm/s)
ρ_s = particle density (g/cm^3)
ρ_l = liquid density (g/cm^3)

The use of Eq. [2] to analyze the experimental results is difficult because of the unknown contact area between individual particles and the melt. The contact area will be strongly dependent on the geometry and change in geometry of the particles as dissolution takes place.

For short times, in which the bulk bath carbon concentration does not change significantly, and the contact area is assumed to be constant, Eq. [2] can be integrated to give the instantaneous particle weight as a function of dissolution time, *i.e.*,

$$W_p = W_i - A\rho_l k(C_s - C_b)t \quad [3]$$

where W_p = particle weight at time t (g)
W_i = initial particle weight (g)

If it is assumed that the particles are spherical, and remain spherical during dissolution while progressively diminishing in diameter, Eq. [3] can be rewritten as,

$$W_p^{1/3} = W_i^{1/3} - (K/\rho_s)^{2/3}\rho_l k(C_s - C_b)t \qquad [4]$$

where K = geometrical constant (2.047).

Acknowledging that the variation of the contact area with time during the dissolution process is unknown, as a first guess, the initial contact area per particle will be assumed to be the surface area of a sphere of the average graphite particle diameter injected into the iron bath. This is a gross approximation and has been done only to give an indication of expected dissolution rates *per particle* for this arbitrary contact area.

In order to obtain some estimate of dissolution rates expected under mass transport conditions, the case of diminishing spherical particles (Eq. [4]) was considered. The mass transport coefficient was estimated from Eq. [1] using dc/dt and $(C_s - C_b)$ values at 85 pct of saturation (the breakaway point on the injection curves for 355 × 106 μm particles at 1450 °C). This gave a k value of 0.12 cm/s, which is reasonable for a gas/particle injection system.[12]

The effects of initial particle size and bath carbon concentration on the times for individual particle dissolution are shown in Figures 8 and 9, respectively. These plots were derived using Eq. [4] above and assume complete contact between the injected particles and the melt at all times during the dissolution process. Figure 8 shows the weight loss as a function of dissolution time for particles of nominal sizes of 100 to 500 micrometers. These calculated results show that the rate of dissolution of the particles decreases with increasing dissolution time due to the diminishing particle/melt contact area. Even for the largest particle size, complete dissolution is expected within approximately 1.5 seconds under the conditions specified (2 pct carbon bath, k = 0.12 cm/s, temperature 1450 °C).

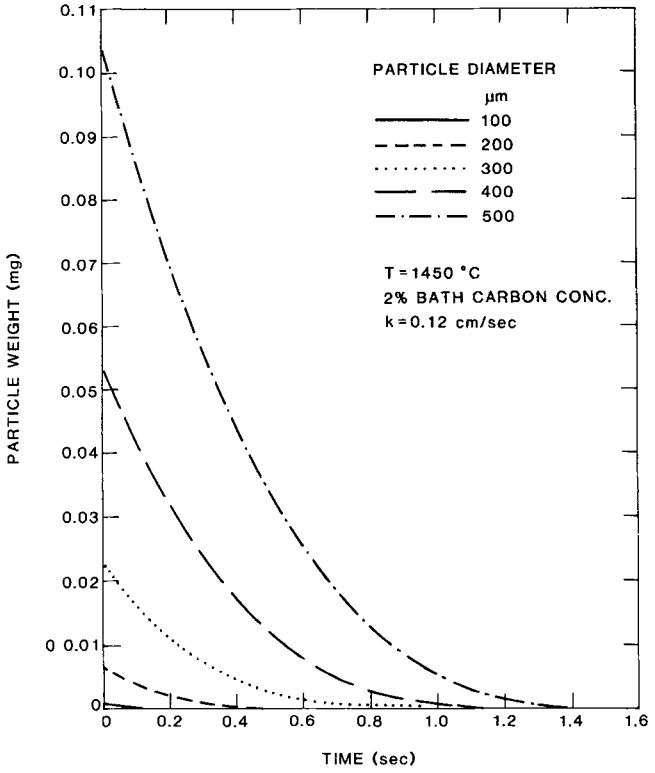

Fig. 8—Calculated effect of graphite particle size on the rate of dissolution.

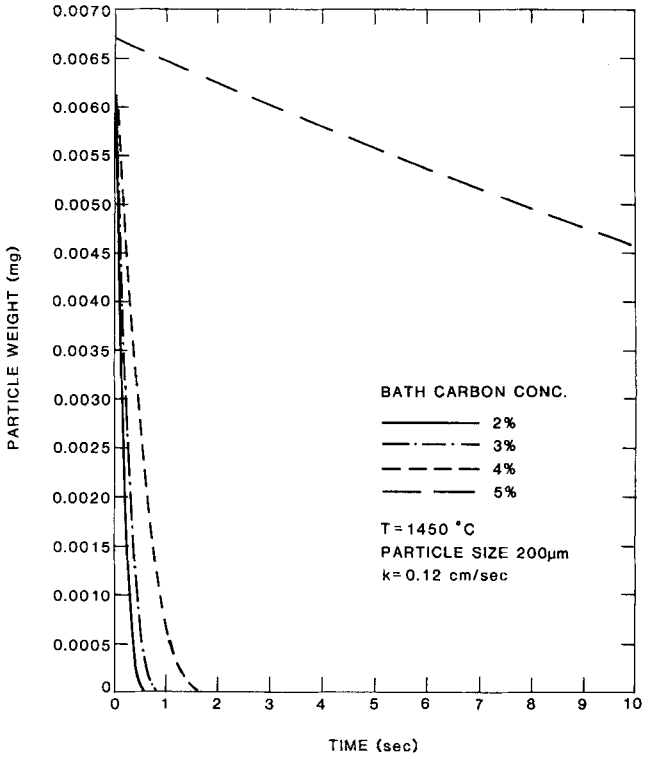

Fig. 9—Calculated effect of bath carbon content on the rate of dissolution of injected graphite.

The effect of increases in the bath carbon content from 2 to 5 pct on the rates of dissolution of particles is shown in Figure 9 (particle diameter 200 micrometers, k = 0.12 cm/s, temperature 1450 °C). This plot shows that beyond a carbon concentration of about 4 pct, the dissolution rates become very slow. This is due to the diminished concentration driving force for the process. At the saturation level, the dissolution must, of course, stop completely.

Overall, these approximate mass transport calculations support the experimental results in that particle dissolution can be expected to occur relatively quickly. The major retarding influence on the rates over the ranges studied is the bath carbon content as saturation is approached. This effect is clearly shown in the experimental results.

Previous work in these laboratories[29] has indicated a plume velocity in the small experimental reactor of about 0.7 m/s. This gives a particle rise time of about 0.08 seconds, which is less than the calculated dissolution times. Therefore, the particles must either dissolve while floating on the surface of the turbulent bath surface or become entrained in the circulating flow. In order to investigate the possibility of entrainment, the flow patterns expected to be generated in the small bottom blown reactor were simulated using the PHOENICS fluid dynamics package. The flow was assumed to be axisymmetric so that the problem could be solved on a two-dimensional polar grid. The sloping wall of the reactor was approximated by a section of a right cone and simulated using the blockage facility of PHOENICS. Boundary

conditions and other details of the simulation procedure are given in Reference 29.

A flow field diagram for the reactor at an injection rate of 4 liters/min is shown in Figure 10. The numerical values of the upward plume velocities average 0.7 to 0.8 m/s, and agree closely with the experimentally inferred plume velocities. Figure 10 indicates strong upward movement from the gas injection port, a surface outward flow to the crucible walls, and a smaller flow down the crucible walls. From this diagram, the downward flow at the crucible walls is estimated at 0.05 to 0.07 m/s. Using Stokes' law, the calculated rise rate of 231 micrometer particles in static Fe/C baths is 0.023 m/s. This suggests that the downward circulation of the bath is probably sufficient to entrain the graphite particles. As dissolution continues, the rise times will decrease with diminishing particle size, and the degree of entrainment will also increase. Thus the combination of initial particle/melt contact (and presumably wetting), and the downward flow at the crucible walls, suggests that the graphite particles are in complete contact with the melt at all times during the dissolution process. Even if some particles do not completely penetrate the bubble interfaces, or are not dragged down into the bath from the surface, then it is likely that the contact area and general bath turbulence level is sufficient to account for the observed high dissolution rates at bath carbon concentration levels below 85 pct of saturation. These effects have been discussed in more detail in other work.[12]

The wettability of carbon by liquid iron/carbon alloys will influence the carbon dissolution rate if the interfacial reaction rate is less than the rate of carbon diffusion away from the interface. In this work it has been assumed that mass transfer within the melt is the rate determining process, and under this assumption, carbon wettability, and/or surface reaction, do not influence the dissolution rate. This tacitly assumes that particle wetting occurs in the system under investigation. Little information is available on the wetting angle of carbon/liquid iron, but it is known[30] that small

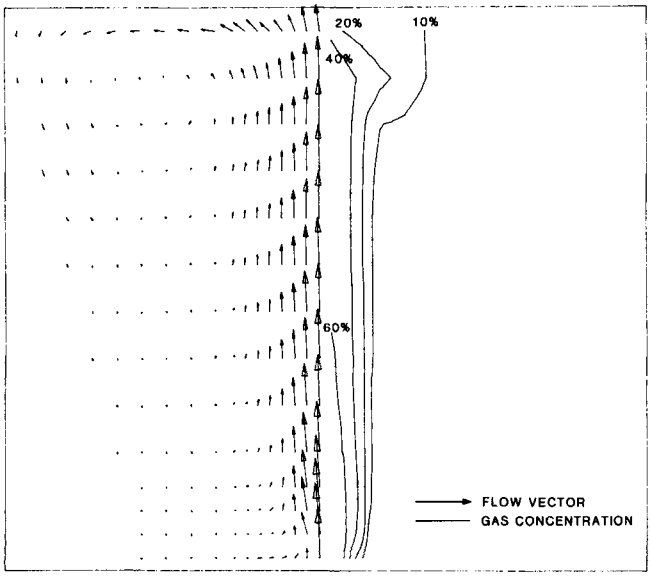

Fig. 10—Flow field diagram for the experimental reactor.

concentrations of surface active elements such as oxygen and sulfur (normally occurring in carbon and coal) considerably reduce the surface tension of liquid iron and hence enhance wettability.

In common with previous investigations, it was found that the sulfur content of the bath retarded the graphite dissolution rates. It has also been found[8] that in sulfur-containing melts the dissolution rates can still satisfy mass transport formulations. If this is so, then the decrease in k values with increasing sulfur concentration must correspond to a change in the kinematic or diffusional characteristics of the melt. While there is little information regarding the effect of sulfur on the kinematic viscosity of Fe/C melts, Heisterkamp and Lohberg[31] found that the chemical diffusion coefficient of carbon in iron at a concentration of 2.5 pct decreased by approximately 20 pct when the sulfur content was increased to 0.12 pct. This suggests that the decrease in the k values may be due to a decrease in carbon diffusivity with increasing sulfur contents. At higher sulfur contents, and with increasing degrees of turbulence, then sulfur may also affect the dissolution rates by influencing the interfacial kinetics of the process. The effect of surface poisoning may also be important. It has also been suggested that the role of sulfur may depend on the carbon type, since the absorption behavior of sulfur will be affected to some extent by the structure of the dissolving surface.

An additional effect of sulfur is to lower the solubility of carbon in iron. For example, at 1500 °C, the addition of 1 pct S to an iron/carbon melt decreases the carbon saturation level from about 5.2 pct to 5.0 pct.[32] Hence sulfur will tend to decrease the concentration driving force for carbon dissolution.

It is not possible to comment on whether the retarding effect of sulfur is due to mass transport, interfacial chemical kinetics, or the positive interaction coefficient in the present investigation; however, it is apparent that any investigation of coal dissolution will have to take into account the coal sulfur content. Sulfur entering the system with the coal may also have a greater retarding effect than the absolute concentrations would indicate as it will be in close proximity and at relatively high concentrations to the actual dissolving surfaces.

IX. CONCLUSIONS

1. An experimental technique has been developed for the bottom injection of particulate materials into Fe/C melts.
2. Particulate graphite dissolution rates in all cases under conditions of varying feed rates, particle sizes, bath temperatures, and carrier gas flows, kept pace with the graphite injection rates up to bath carbon concentrations within about 85 pct of saturation.
3. The dissolution results and approximate rate calculations based on the assumption of mass transport limitations are in qualitative agreement.
4. Flow simulations using the PHOENICS fluid dynamics package has suggested that the injected particles are completely entrained in the gas-stirred circulating melt.
5. Bath sulfur has a retarding effect on the graphite dissolution rates.

APPENDIX

Calculation of particle velocities in vertical gas conveying, from Chandok and Pei[27]

$$\frac{U_{s(o)}}{U_\alpha} = 1 + C_1 \rho^{-C_{2M}} \quad [1]$$

where $U_{s(o)} = U_{g(o)} - U_{p(o)}$ [2]

$U_{g(o)}$ = gas velocity at pipe center line (m · s^{-1})

$U_{p(o)}$ = particle velocity at pipe center line (m · s^{-1})

$U_{s(o)}$ = slip velocity at pipe center line (m · s^{-1})

U_α = particle settling velocity (m · s^{-1})

$C_1 = 16.78/\mathrm{Re}_p^{(0.7)}$

$C_2 = 1.25/\mathrm{Re}_p^{(0.38)}$

$\mathrm{Re}_p = \dfrac{\rho_g U_{s(o)} d}{U_g}$

ρ_g = gas density (kg · m^3)

d = particle diameter (m)

U_g = gas viscosity (Pa-s)

For low mass loadings, *i.e.*, $M^* < 1.0$, the turbulent gas velocity profile may be approximated by a 1/7th power law, *i.e.*,

$$U_{g(r)} = U_{g(o)}\left(\frac{R - r}{R}\right)^{1/7} \quad [3]$$

where $U_{g(r)}$ = velocity of gas at radial position r (m · s^{-1})

r = radial position (m)

R = pipe radius (m)

The average gas velocity is given by,

$$\overline{U}_g = \frac{U_{g(o)}}{R}\int_0^R \left(\frac{R - r}{R}\right)^{1/7} dr = \frac{7}{8} U_{g(o)} \quad [4]$$

Similarly, the solids velocity profile may be approximated to a power law developed by Soo[28] for vertical conveying,

$$U_{p(r)} = [U_{p(o)} - U_{p(R)}]\left[\frac{R - r - d/2}{R - d/2}\right]^{1/m} + U_{p(R)} \quad [5]$$

where $U_{p(R)}$ = particle velocity at the wall (m · s^{-1})

$m = 3.78 - 7.0 \times 10^{-3}\mathrm{Re}_{p(o)}$[27]

$\mathrm{Re}_{p(o)} = \dfrac{\rho_g U_{s(o)d}}{U_g}$

The calculation of $U_{p(R)}$ usually requires knowledge of the appropriate diffusivities, and most importantly, an understanding of the particle/wall interaction. For the purpose of these calculations, $U_{p(R)}$ may be approximated by,[27]

$$U_{p(R)} = 0.68 U_{p(o)} \quad [6]$$

Similarly, average particle velocity $\overline{U}_p$ is given by,

$$\overline{U}_p = \frac{[U_{p(o)} - U_{p(R)}]}{(R - d/2)}\int_0^{R-d/2}\left[\frac{R - r - d/2}{R - d/2}\right]^{1/m} + U_{p(R)}$$

$$= \frac{U_{p(o)} - U_{p(R)}}{(1 + 1/m)} + U_{p(R)} \quad [7]$$

The calculation method involves estimating the axial slip velocity, $U_{s(o)}$, from Eq. [1] and the axial gas velocity, $U_{g(o)}$, from Eq. [4].

Since

$$U_{s(o)} = U_{g(o)} - U_{p(o)} \quad [8]$$

the axial particle velocity, $U_{p(o)}$, is known and the particle velocity at the tube wall, $U_{p(R)}$, can be calculated from Eq. [6]. The average particle velocity can then be calculated using Eq. [7].

ACKNOWLEDGMENTS

The authors acknowledge helpful discussions with Dr. L. Pullum regarding particle hydraulic transport. The financial support of CRA Ltd. is gratefully acknowledged.

REFERENCES

1. S. Eketorp: *Extraction Metallurgy '81*, Institution of Mining and Metallurgy, London, 1981, pp. 184-92.
2. J. K. Wright, W. T. Denholm, and R. A. McClelland: NERDDC Project End of Grant Report, 1984, 125 p.
3. G. D. Spenceley and P. J. Kreijger: *Ironmaking and Steelmaking*, 1983, vol. 10(3), pp. 114-23.
4. L. von Bogdandy, K. Brotzmann, and E. Fritz: *Steelmaking Proceedings*, 1982, vol. 65, pp. 287-95.
5. R. G. Olsson, V. Komp, and T. F. Perzak: *Trans. TMS-AIME*, 1966, vol. 236, pp. 426-29.
6. M. Kosaka and S. Minowa: *Trans. I.S.I.J.*, 1968, vol. 8(6), pp. 392-400.
7. L. Kalvelage, J. Markert, and J. Potschke: *Arch. Eisenhüttenwes.*, 1979, vol. 50(3), pp. 107-10.
8. S. O. Ericsson and P. O. Melberg: *Scand. J. Met.*, 1981, vol. 10, pp. 15-18.
9. V. A. Grigoryan and V. P. Karshin: *Russian Metallurgy*, 1972, pp. 57-59.
10. J. Szekely, T. Lehner, and C. W. Chang: *Ironmaking and Steelmaking*, 1979, vol. 6, pp. 2825-33.
11. J. K. Wright and W. T. Denholm: *Extractive Metallurgy Symposium, Aus.I.M.M.*, Melbourne, Vic., 1984, pp. 323-29.
12. T. Lehner: *Scaninject*, Luleå, Sweden, 1977, vol. 11, pp. 1-47.
13. R. P. Singh and M. J. McNallan: *Metall. Trans. B*, 1983, vol. 14B, pp. 425-34.
14. T. A. Engh, K. Larsen, and K. Venas: *Ironmaking and Steelmaking*, 1979, vol. 6, pp. 268-73.
15. Y. Ozawa and K. Mori: *Trans. ISIJ*, 1983, vol. 23, pp. 671-75.
16. D. N. Ghosh and K. W. Lange: *Ironmaking and Steelmaking*, 1982, vol. 3, pp. 136-41.
17. Y. Ozawa and K. Mori: *Trans. ISIJ*, 1983, vol. 23, pp. 769-74.
18. L. R. Farias and D. G. C. Robertson: *Proceedings of 3rd Process Technology Conference*, Luleå, Sweden, 1980, pp. 8.1-8.10.
19. G. A. Irons and B. H. Tu: *Proceedings of Scaninject III Conference*, Luleå, Sweden, 1983, pp. 11.1-11.29.
20. L. R. Farias and G. A. Irons: *Metall. Trans. B*, 1985, vol. 16B, pp. 211-25.
21. E. Kimura: *Trans. ISIJ*, 1983, vol. 23, pp. 522-29.
22. N. A. Voronova: Moscow, *Metallurgiya*, 1973, pp. 237-42.
23. G. M. Paliy and M. F. Sidorenko: Moscow, *Metallurgiya*, 1972, pp. 177-83.
24. T. A. Engh, A. Sandberg, A. Hultkvist, and L. G. Norberg: *Scand. J. Met.*, 1972, vol. 1, p. 103.
25. K. Narita, T. Makino, H. Matsumoto, and K. Ogawa: *Tetsu-to-Hagané*, 1983, vol. 69, p. 392.
26. Y. Ozawa, K. Suzuki, and K. Mori: *Tetsu-to-Hagané*, 1983, vol. 69, p. 753.
27. S. S. Chandok and D. C. T. Pei: *First Int. Conf. on the Pneumatic Transport of Solids in Pipes*, University of Waterloo, ON, Canada, 1971, pp. B5-53.
28. S. L. Soo: *First Int. Conf. on the Hydraulic Transport of Solids in Pipes*, University of Warwick, Cranfield, Bradford, England, 1971, pp. A1-1.
29. M. P. Schwarz, J. K. Wright, B. R. Baldock, and B. Addison-Smith: CHEMECA '87, The 15th Australian Chemical Engineering Conference, Melbourne, 1987, Paper 102, 8 pages.
30. I. Barin, M. Modigell, and F. Sauert: *Metall. Trans. B*, 1987, vol. 18B, pp. 347-54.
31. F. Heisterkamp and K. Lohberg: *Arch. Eisenhüttenw.*, 1966, vol. 37, pp. 813-19.
32. *The Making, Shaping and Treating of Steel*, H. E. McGannon, ed., United States Steel, 1964.